Reflection asymmetric shell model for octupole-deformed nuclei

Y. S. Chen[1,2] and Z. C. Gao[1]
[1]*China Institute of Atomic Energy, P.O. Box 275(18), Beijing 102413, China*
[2]*Institute of Theoretical Physics, Academia Sinica, Beijing 100080, China*
(Received 5 July 2000; published 20 December 2000)

The reflection asymmetric shell model has been established by means of the variational procedure and the projection method to describe the high spin states of octupole deformed nuclei. The $Q\cdot Q$ forces of quadrupole, octupole, and hexadecapole as well as the monopole and quadrupole pairings are included in the Hamiltonian. The shell model space is spanned by a selected set of the simultaneous angular momentum- and parity-projected BCS multiquasiparticle states which are intrinsically deformed. The general features of rotational octupole bands in even-even nuclei can be interpreted and reproduced by the present model, and the calculated results for the Ra isotopes are in good agreement with the experimental data.

DOI: 10.1103/PhysRevC.63.014314 PACS number(s): 21.60.Cs, 21.60.Ev, 21.10.Re, 27.90.+b

I. INTRODUCTION

With the first observation of low-lying negative-parity states by the Berkeley group in the 1950's [1,2], the possibility arose that some nuclei might have a shape asymmetric under reflection. The sequence of rotational states with alternating parity I^+, $(I+1)^-$, $(I+2)^+$, . . . , here I is even integer number, was first observed in ^{218}Ra [3] and ^{222}Th [4] in the 1980's. These rotational bands provide the evidence for the strong octupole correlation or even the static octupole deformation. In the last decade, a flurry of experimental and theoretical discoveries (reviewed, e.g., in Refs. [5,6]) have provided new indications of the reflection-asymmetric octupole deformation. The rotational bands of states with alternating parity have been observed up to very high spin [7–9], particularly in nuclei around ^{224}Ra. These band structures are analogous to those of asymmetric molecules such as HCl and may be expected for nuclei with octupole deformation. For many of these nuclei there exist intrinsic electric dipole moments giving rise to strong electric-dipole transitions connecting states of opposite parity. The striking behavior of the octupole bands highlights the nuclear reflection asymmetry and has attracted much interest over the years.

A diversified models have been developed for the study of the properties of octupole bands, refer to Ref. [6], and references therein. Among those microscopic approaches the cranked shell model (CSM) is one of the most useful models to describe the properties of high spin states in octupole deformed nuclei [10]. Despite the success of the CSM in the description of high spin states, its disadvantage is clear for the fact that angular momentum is not a good quantum number, but instead a classical term, the rotational frequency is employed. Also the parity is not a good quantum number when the octupole deformation onsets. Therefore the CSM calculations cannot be directly compared with the measured energy levels of rotational bands as well as the transition rates between band states. Moreover, the residual interactions between the quasiparticle configurations are not properly considered in the CSM and thus the detailed description of the wave functions of rotational states by the CSM becomes somewhat in question. The purpose of the present work is to establish a new microscopic model, called the reflection asymmetric shell model (RASM), in order to describe the high spin states in octupole deformed nuclei. The basic assumption of the CSM, clearly a key advantage, is that the picture of quasiparticles moving in the deformed rotating mean field can provide a good basis to describe the properties of rotational bands. This advantage has been taken in the new model by introducing a selected set of the intrinsically deformed multiquasiparticle states to form the basis to achieve a good and sufficient truncation of the shell model space. The disadvantages of the CSM mentioned above, namely, no good parity, no good angular momentum, and no residual interaction between quasiparticle configurations, are removed in the RASM by carrying out the projection procedure and introducing the $Q\cdot Q$ forces. In the RASM, the basis on which the spherical Hamiltonian will be diagonalized are the eigenstates of angular momentum and parity obtained by projecting the intrinsic reflection asymmetric, octupole deformed, multiquasiparticle states onto good angular momentum and good parity. We will see that the shell model space spanned by the states of only three major shells for protons and neutrons is large enough for the RASM calculation of the low-lying octupole bands in heavy octupole deformed nuclei, and that all the general features of octupole bands can be reproduced and the calculated results for the Ra isotopes are in good agreement with the experimental data.

Elliott was the first to point out the advantage of a deformed (intrinsic) many-body basis and develop the SU(3) shell model [11] for sd-shell nuclei by using the group theory. The projected shell model (PSM) [12,13], of which the basis is a selected set of the quadrupole deformed Nilsson + BCS multiquasiparticle states, can be considered to be a natural extension of the SU(3) shell model to heavier systems. The basis of both models violates the symmetry of rotation but it can be recovered by angular momentum projection. For an intrinsic octupole and simultaneously quadrupole deformed system, the case that the present model deals with, not only the rotation but also the reflection symmetries are violated and thus the parity projection is required in addition to angular momentum projection to recover the symmetries. The model is an extension of the projected shell model [12,13] by including the parity projection in addition to angular momentum projection and the octupole and hexa-

decapole interactions in the Hamiltonian.

A brief description and derivation of the theory is presented in Sec. II. In Sec. III the general features of rotational octupole bands are discussed and interpreted by the model. In Sec. IV the calculated results of the octupole yrast bands for ^{222,224,226,228,230}Ra are shown and compared with the experimental data. A summary is in Sec. V.

II. THE MODEL

A. The eigenvalue equation

Let us consider an intrinsic deformed state $|\Phi\rangle$, precisely with octupole, quadrupole, and hexadecapole deformations, which is not an eigenstate of the angular momentum and parity operators. Because of the invariance of rotation and reflection of the spherical shell model Hamiltonian one has the identical equations

$$H=\hat{R}^{\dagger}(\Omega)H\hat{R}(\Omega)=\hat{P}^{\dagger}H\hat{P}=\hat{R}^{\dagger}(\Omega)\hat{P}^{\dagger}H\hat{P}\hat{R}(\Omega), \quad (1)$$

where $R(\Omega)$ is the rotation operator which has the explicit form, $e^{-\imath\alpha\hat{J}_z}e^{-\imath\beta\hat{J}_y}e^{-\imath\gamma\hat{J}_z}$, Ω represents a set of Euler angles ($\alpha,\gamma=[0,2\pi]$ and $\beta=[0,\pi]$), and $\hat{P}$ is the parity operator, and it is obvious that there is the commutation relation

$$[\hat{P},\hat{R}(\Omega)]=0. \quad (2)$$

Using the generator coordinate Ω we may construct a wider class of states by forming a trial wave function

$$|\Psi\rangle=\int d\Omega F_1(\Omega)\hat{R}(\Omega)|\Phi\rangle+\int d\Omega F_2(\Omega)\hat{P}\hat{R}(\Omega)|\Phi\rangle, \quad (3)$$

where $F_1(\Omega)$ and $F_2(\Omega)$ are functions to be determined by minimizing the energy expectation value. $F_1(\Omega)$ and $F_2(\Omega)$ can be expanded in terms of the D function

$$F_1(\Omega)=\sum_{IMK}\frac{2I+1}{8\pi^2}F^I_{1,MK}D^I_{MK}(\Omega),$$

$$F_2(\Omega)=\sum_{IMK}\frac{2I+1}{8\pi^2}F^I_{2,MK}D^I_{MK}(\Omega). \quad (4)$$

Replacing $F_1(\Omega)$ and $F_2(\Omega)$ in Eq. (3) by the expressions of Eq. (4), we obtain

$$|\Psi\rangle=\sum_{IMK}\{F^I_{1,MK}P^I_{MK}|\Phi\rangle+F^I_{2,MK}\hat{P}P^I_{MK}|\Phi\rangle\}$$

$$=\sum_{IMKp}F^{Ip}_{MK}P^pP^I_{MK}|\Phi\rangle, \quad (5)$$

where P^p is the parity projection operator,

$$P^p=\frac{1}{2}(1+p\hat{P}), \quad (6)$$

with $p=\pm1$, and P^I_{MK} is the angular momentum projection operator,

$$P^I_{MK}=\frac{2I+1}{8\pi^2}\int d\Omega D^I_{MK}(\Omega)\hat{R}(\Omega). \quad (7)$$

To obtain the second identity in Eq. (5) we have used the definition

$$F^{Ip}_{MK}\equiv F^I_{1,MK}+pF^I_{2,MK}. \quad (8)$$

The coefficients F^{Ip}_{MK} play the role of the variational parameters taking the place of the variational functions $F_1(\Omega)$ and $F_2(\Omega)$ in Eq. (3). Then the variational procedure can be carried out by using the trial wave function of Eq. (5). For that some useful properties of the parity and angular momentum projection operators are

$$P^{p\dagger}=P^p,$$

$$P^{p'}P^p=\delta_{p'p}P^p,$$

$$P^{I\dagger}_{MK}=P^I_{KM},$$

$$P^{I'}_{K'M'}P^I_{MK}=\delta_{II'}\delta_{MM'}P^I_{K'K}. \quad (9)$$

It is straightforward to obtain the expressions of the expectation value of the Hamiltonian and the normal product $\langle\Psi|H|\Psi\rangle$ and $\langle\Psi|\Psi\rangle$ by using Eq. (9).

$$\langle\Psi|H|\Psi\rangle=\sum_{IKK'pM}F^{Ip*}_{MK'}F^{Ip}_{MK}\langle\Phi|HP^pP^I_{K'K}|\Phi\rangle,$$

$$\langle\Psi|\Psi\rangle=\sum_{IKK'pM}F^{Ip*}_{MK'}F^{Ip}_{MK}\langle\Phi|P^pP^I_{K'K}|\Phi\rangle. \quad (10)$$

According to the variational equation

$$\delta\langle\Psi|H|\Psi\rangle-E\,\delta\langle\Psi|\Psi\rangle=0, \quad (11)$$

we obtain the eigenvalue equation which the wave function, more precisely the coefficients F^{Ip}_{MK} fulfill

$$\sum_K F^{Ip}_{MK}(\langle\Phi|HP^pP^I_{K'K}|\Phi\rangle-E\langle\Phi|P^pP^I_{K'K}|\Phi\rangle)=0. \quad (12)$$

It is easy to see that for each value of E in Eq. (12) there exist a definite set of values of I,M and p for which F^{Ip}_{MK} is nonzero and the other $F^{I'p'}_{M'K}$ vanishes. Thus the summation over I, M, and p in Eq. (5) actually drops away, as seen in Eq. (12). In other words, this means that $|\Psi\rangle$ becomes an eigenstate of angular momentum and parity. Both the rotation and reflection symmetries violated in the original intrinsic state $|\Phi\rangle$ are thus recovered in the new state $|\Psi\rangle$ in the laboratory frame.

B. The configuration mixing

However, so far only one single intrinsic state $|\Phi\rangle$ has been considered in the above discussion. It is necessary to consider the configuration mixing in order to deal with the interaction between various unperturbed bands. We consider a set of deformed multiquasiparticle states $\{|\Phi_\kappa\rangle\}$ instead of the single state $|\Phi\rangle$, where κ denotes the quasiparticle configurations, and then the trial superposition $|\Psi\rangle$ becomes in a more generalized form

$$|\Psi\rangle=\sum_{IMK\kappa p} F^{Ip}_{MK} P^p P^I_{MK\kappa}|\Phi_\kappa\rangle. \tag{13}$$

The $\{P^pP^I_{MK}|\Phi_\kappa\rangle\}$ is the set of simultaneously angular momentum- and parity-projected multiquasiparticle states which forms the shell model space and allows the configuration mixing. By performing the similar variational procedure one obtains the final eigenvalue equation

$$\sum_{K\kappa}\{\langle\Phi_{\kappa'}|HP^pP^I_{K'K}|\Phi_\kappa\rangle-E^{Ip}\langle\Phi_{\kappa'}|P^pP^I_{K'K}|\Phi_\kappa\rangle\}F^{Ip}_{MK\kappa}=0, \tag{14}$$

and the normalization condition

$$\sum_{K\kappa' K\kappa} F^{Ip*}_{MK'\kappa'}\langle\Phi_{\kappa'}|P^pP^I_{K'K}|\Phi_\kappa\rangle F^{Ip}_{MK\kappa}=1. \tag{15}$$

According to Eq. (14), $|\Psi\rangle$ in Eq. (13) is still an eigenstate of both angular momentum and parity and thus the summation over I, M, and p contains only one term, but the summation over κ leads to the configuration mixing. Also from Eq. (14), we can see that the coefficient $F^{Ip}_{MK\kappa}$ is independent of magic quantum number, so the subscript M can be omitted. It is noted that Eq. (14) is valid for any nuclear shape, but in the present study we only consider the case of axial symmetry. Once $\langle\Phi_{\kappa'}|HP^pP^I_{K'K}|\Phi_\kappa\rangle$ and $\langle\Phi_{\kappa'}|P^pP^I_{K'K}|\Phi_\kappa\rangle$ are available, the eigenvalues E^{Ip} of H together with the wave functions can be calculated from Eq. (14).

C. The Hamiltonian

The Hamiltonian is

$$H=H_0-\frac{1}{2}\sum_{\lambda=2}^{4}\chi_\lambda\sum_{\mu=-\lambda}^{\lambda}Q^\dagger_{\lambda\mu}Q_{\lambda\mu}-G_0P^\dagger_{00}P_{00}-G_2\sum_{\mu=-2}^{2}P^\dagger_{2\mu}P_{2\mu}, \tag{16}$$

where H_0 is the spherical single particle Nilsson Hamiltonian and

$$Q_{\lambda\mu}=\sum_{\alpha,\beta}\langle\alpha|\rho^2Y_{\lambda\mu}|\beta\rangle c^\dagger_\alpha c_\beta, \tag{17}$$

$$P^\dagger_{00}=\frac{1}{2}\sum_\alpha c^\dagger_\alpha c^\dagger_{\bar\alpha}, \tag{18}$$

$$P^\dagger_{2\mu}=\frac{1}{2}\sum_{\alpha,\beta}\langle\alpha|\rho^2Y_{2\mu}|\beta\rangle c^\dagger_\alpha c^\dagger_{\bar\beta}, \tag{19}$$

where $c^\dagger_\alpha$ and c_α are the single particle creation and annihilation operator, respectively, and $\rho=\sqrt{m\omega_0/\hbar}r$. This Hamiltonian includes quadrupole-quadrupole ($\lambda=2$), octupole-octupole ($\lambda=3$), and hexadecapole-hexadecapole ($\lambda=4$) interactions which leads to the quadrupole, octupole, and hexadecapole deformations, respectively. The coupling constants of the $Q_\lambda\cdot Q_\lambda$ forces, χ_λ in Eq. (16), may be determined inconsistent to the nuclear deformations ϵ_λ (similar to Ref. [13]), and can be calculated by the expressions

$$\chi_{2,\tau\tau'}=\frac{\frac{2}{3}\sqrt{\frac{4\pi}{5}}\epsilon_2\hbar\omega_\tau\hbar\omega_{\tau'}}{\hbar\omega_n\langle Q_{20}\rangle_n+\hbar\omega_p\langle Q_{20}\rangle_p},$$

$$\chi_{3,\tau\tau'}=\frac{-\sqrt{\frac{4\pi}{7}}\epsilon_3\hbar\omega_\tau\hbar\omega_{\tau'}}{\hbar\omega_n\langle Q_{30}\rangle_n+\hbar\omega_p\langle Q_{30}\rangle_p},$$

$$\chi_{4,\tau\tau'}=\frac{-\sqrt{\frac{4\pi}{9}}\epsilon_4\hbar\omega_\tau\hbar\omega_{\tau'}}{\hbar\omega_n\langle Q_{40}\rangle_n+\hbar\omega_p\langle Q_{40}\rangle_p}, \tag{20}$$

where $\langle\cdots\rangle$ means the expectation value with respect to the BCS vacuum state, $\tau(\tau')$ refers to neutron or proton. The present multipole plus pairing force model works surprisingly well for octupole and quadrupole deformed nuclei despite its simplicity. Nevertheless, the neutron-proton interaction presents only in the (particle-hole type) $Q\cdot Q$ force, which might be too restrictive.

The Hamiltonian (16) is then diagonalized within the shell model space spanned by a selected set of the simultaneously parity- and angular momentum-projected BCS multiquasiparticle states. The quasiparticle configurations employed in the present calculations for even-even nuclei include the vacuum, two neutrons, two protons, and four quasiparticle states, $\|0\rangle$, $a^\dagger_{\mu1}a^\dagger_{\mu2}\|0\rangle$, $a^\dagger_{\pi1}a^\dagger_{\pi2}\|0\rangle$, $a^\dagger_{\mu1}a^\dagger_{\mu2}a^\dagger_{\pi1}a^\dagger_{\pi2}\|0\rangle$, where μ's (π's) denote the neutron (proton) Nilsson quantum numbers which run over properly selected low-lying quasiparticle states.

D. Parameters

The monopole pairing strength parameter may be obtained by the expression

$$G_0=\left(g_1\mp g_2\frac{N-Z}{A}\right)/A, \tag{21}$$

where $g_1=17.52$ and $g_2=10.83$ was taken in the present calculation of the Ra region, and the minus (plus) sign stands for neutron (proton). The strength of the quadrupole pairing

TABLE I. The deformation parameters used for the calculations of the Ra isotopes.

Nucleus	ϵ_2	ϵ_3	ϵ_4
^{222}Ra	0.07	0.071	−0.12
^{224}Ra	0.08	0.071	−0.12
^{226}Ra	0.08	0.071	−0.12
^{228}Ra	0.10	0.061	−0.10
^{230}Ra	0.12	0.055	−0.10

may be calculated from $G_2 = fG_0$, usually $f = 0 \sim 0.2$. In the present calculations we set $f = 0$, namely no quadrupole pairing, since it is not important for the case of rather small quadrupole deformation, as in the Ra region. The three major shells of $N = 5,6,7$ for neutrons and $N = 4,5,6$ for protons are included to calculate the Nilsson single particle states. The Nilsson potential parameters used are $(\kappa, \mu) = (0.058, 0.44)$ for neutron and (0.048,0.69) for proton shells. The spherical single particle energies of the present Nilsson potential are similar to those of the Woods-Saxon potential (Ref. [14], and references therein). The level spectra become quite similar for the two potentials in the presence of both quadrupole and octupole deformations, especially the pronounced energy gaps appearing at neutron numbers $N = 138$ and 132 and proton number $Z = 88$ which characterize the mass region. The deformation parameters including the quadrupole ϵ_2, the octupole ϵ_3 and the hexadecapole ϵ_4 are chosen to have reasonable values, and these values for Ra isotopes as listed in Table I are similar to those given in Refs. [6,14], and references therein, except a rather larger ϵ_4 as discussed in Sec. IV.

III. GENERAL FEATURES OF ROTATIONAL OCTUPOLE BANDS

By examining the behavior of all of the yrast octupole bands observed in the Ra region a number of interesting common features clearly stand out, which are different from those of the normal rotational bands observed in nonoctupole but quadrupole deformed nuclei: the specific sequence of states $0^+, 1^-, 2^+, 3^-, \ldots$; the significant parity splitting at low spins; the quenching of the parity splitting by rotation; the absence of the sharp band crossing. All these general features characteristic of octupole deformed nuclear system may be interpreted based on the framework of the RASM.

A. The specific sequence of states

The sequence of states with even-spin, positive parity and odd-spin, negative parity, namely, $I^+, (I+1)^-, (I+2)^+, \ldots$, was found in all the observed rotational yrast octupole bands in the even-even octupole deformed nuclei in the $A = 140$, 220, and 240 mass regions. The sequence was accepted in the literature as an observed general feature associated with the rotational motion of the octupole deformed system, but has not been well studied. The mathematic logic of the RASM provides the insight into the origin of the sequence. If the band mixing is neglected, the energies of the g.s. band can be evaluated by

$$E^{Ip} = \frac{\langle HP^p P^I_{00} \rangle}{\langle P^p P^I_{00} \rangle}, \tag{22}$$

where $\langle \cdots \rangle$ stands for the expectation value with respect to the BCS vacuum. For the case of axial symmetry, the integration in Eq. (7) becomes one dimensional, precisely the angle β, and $\hat{R}(\Omega)$ becomes $\hat{r}(\beta) = e^{-\imath \beta j_y}$, and then one obtains

$$E^{Ip} = \frac{(1 + p(-1)^I) \int_0^\pi d\beta \sin\beta d^I_{00}(\beta) \langle H\hat{r}(\beta) \rangle}{(1 + p(-1)^I) \int_0^\pi d\beta \sin\beta d^I_{00}(\beta) \langle \hat{r}(\beta) \rangle}. \tag{23}$$

In Eq. (23) the factor $[1 + p(-1)^I]$ should not be zero otherwise the equation is meaningless, namely, the expression of the energy becomes uncertain and therefore I must be even integer number for $p = 1$ and odd integer number for $p = -1$. Thus the allowable values of I and p are even-spin, positive parity and odd-spin, negative parity, and then Eq. (23) is deduced to be

$$E^{Ip} = \frac{\int_0^\pi d\beta \sin\beta d^I_{00}(\beta) \langle H\hat{r}(\beta) \rangle}{\int_0^\pi d\beta \sin\beta d^I_{00}(\beta) \langle \hat{r}(\beta) \rangle}. \tag{24}$$

It is interesting to note that in the case of reflection symmetry $\langle \hat{O}\hat{r}(\beta) \rangle = \langle \hat{O}\hat{r}(\pi - \beta) \rangle$ and $d^I_{00}(\beta) = (-1)^I d^I_{00}(\pi - \beta)$, where $\hat{O} = 1$ or H, the E^{I-} states with odd I no longer exist since both the numerator and the denominator in Eq. (24) vanishes, and only possible are the states of $0+, 2+, \ldots$, the sequence of the yrast rotational states observed in even-even nonoctupole but quadrupole deformed nuclei.

B. The parity splitting at low spins

The parity splitting observed in almost all the octupole deformed nuclei measures to the extent to which the odd-spin, negative parity level of spin I has an excitation energy located higher than the average of those of the two neighboring even-spin, positive parity states with respective spins $I-1$ and $I+1$. This quantity is one of the unique features of the presence of octupole modes and has attracted much interest over the years, and it was called ''the energy displacement'' in Ref. [10] and is similar to the quantity ''signature splitting index'' defined in Ref. [17] and the quantity ''staggering'' defined in Ref. [18]. The parity splitting characteristic of the octupole deformation can be reproduced by the RASM. Figure 1 presents the parity splittings for the yrast octupole bands calculated as a function of the octupole deformation ϵ_3 with fixed quadrupole and hexadecopole deformations $\epsilon_2 = 0.08$ and $\epsilon_4 = -0.12$. The Nilsson potential and the pairing parameters given in Sec. III are used to calculate Fig. 1, and these parameters are suitable for the calculations of the Ra isotopes, as will be seen below. Therefore the tendency of the parity splittings presented in Fig. 1 reflects in

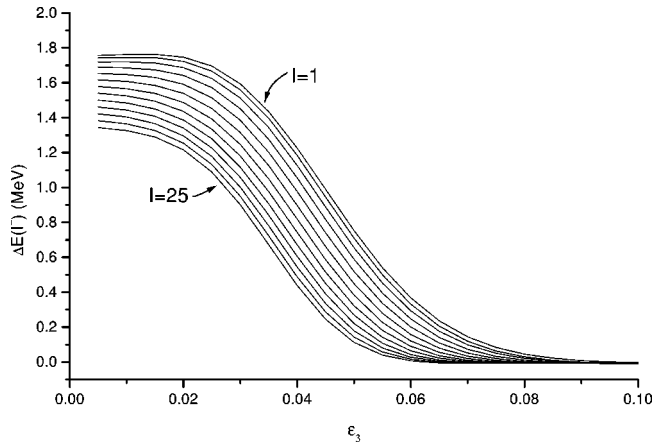

FIG. 1. The parity splitting in the yrast bands versus the octupole deformation ϵ_3 calculated for each odd spin I^- from 1^- to 25^-. The parity splitting is defined as the quantity $\Delta E(I^-) = E(I^-) - \{E[(I-1)^+] + E[(I+1)^+]\}/2$. The parameters used in the calculation refer to the text.

somewhat extent the situation in the Ra region. It can be seen from Fig. 1 that the parity splitting decreases with the increasing ϵ_3 at a given spin. At low odd spins, 1^-,3^-, and 5^-, the parity splitting decreases from $\sim$1000 keV at $\epsilon_3 = 0.04$ to $\sim$200 keV at $\epsilon_3 = 0.07$ which is typical value of the octupole deformation for the Ra isotopes. The parity splitting at low spins is sensitive to the change of the octupole deformation. In fact, when ϵ_3 becomes large the strength of the octupole-octupole force in the Hamitonian χ_3 becomes stronger so that the negative parity band lies lower in energy, closer to the positive parity yrast band. Thus the parity splitting may reduce to zero for a large enough octupole deformation. It is interesting to note from Fig. 1 that at the typical value of the octupole deformation, $\epsilon_3 \sim 0.07$, for the light Ra isotopes the parity splitting is about 200 keV at spin 1^- which accounts for the observed parity splitting.

C. The quenching of the parity splitting

Another striking feature shown in Fig. 1 is that the parity splitting decreases with increasing spin at a given value of ϵ_3, which is so-called the quenching of the parity splitting. Indeed, although the parity splitting exists at low spins in almost all the observed rotational octupole bands in even-even octupole nuclei, but it decreases with the increasing spin and vanishes after a critical spin. This means that the parity splitting can be significantly quenched by the fast rotation. There exists a critical spin I_c where the splitting vanishes and the negative and the positive parity states become interleaved. It is seen from Fig. 1 that the critical spin I_c may be quite large, $\sim 25^-$, for a rather small octupole deformation $\epsilon_3 = 0.06$, and small, $\sim 3^-$, for a rather large octupole deformation $\epsilon_3 = 0.09$. And it will be seen in Sec. IV that this estimation is qualitatively valid for the case of the Ra isotopes.

D. The absence of the sharp band crossing

The majority of octupole rotational bands observed in the light actinides exhibit smooth behavior, showing no sharp band crossing up to very high spins, while the band crossing is expected to present at a much lower spin in nonoctupole deformed nuclei. Calculations based on the cranked reflection asymmetric WS model reproduce the absence of the sharp band crossing [10]. When the mean field is cranked in order to describe high spin states, the angular momentum is much more homogeneously distributed, namely, fragmented, over the rotational quasiparticles with and without octupole deformation. The sufficient mixing of the intruder shells with the valence orbitals can be induced by even a small octupole deformation, and is responsible for the fragmentation of angular momentum. It is obvious that such an effect of the octupole deformation on the fragmentation of angular momentum of the quasiparticles is fully included in the RASM, and thus the smooth behavior of the yrast octupole bands can be reproduced by the RASM calculation, as shown in Fig. 2.

IV. CALCULATIONS FOR THE Ra ISOTOPES

The yrast octupole bands, the energy versus spin, for ^{222,224,226,228,230}Ra calculated up to spin 26 are shown and compared with the experimental data [9] in Fig. 2. The deformation parameters (ϵ_2, ϵ_3, ϵ_4) used for the calculations of the deformed quasiparticle basis states are listed in Table I. The other Nilsson potential and the pairing force parameters are the same for all the calculations in this work and as given in Sec. III. It is seen that for the overall behavior of the rotational octupole bands the agreement between the experiment and theory is remarkable. It is noticed that with the shell model space of three major shells for protons and neutrons and only small changes of the deformation parameters the present calculations are able to reproduce the experiments for all the yrast rotational octupole bands observed in the even-even $^{222-230}$Ra nuclei. It is well known that the hexadecapole deformation is large in the light actinides. In the present calculations a large ϵ_4 value is employed for better reproducing the experimental data of the yrast bands. It is instructive to notice that the deformation parameters listed in Table I describe an octupole shape that is closer to the cluster picture of the ^{208}Pb-like plus ^{14}C-like with a fat neck. A detailed discussion of this point is beyond the scope of the present paper and will be studied in the forthcoming paper.

The parity splittings at low spins for all these nuclei are well reproduced by the present calculations, as seen in Fig. 2. The calculated parity splittings at spin 1^-, $\Delta E[1^-) = E(1^-) - (E(0^+) + E(2^+)]/2$, for the Ra isotopes are plotted versus the mass number A and compared with the experimental data in Fig. 3. It is seen that the parity splitting has almost a constant value of $\sim$200 keV for $A = 222$, 224, and 226, but increases suddenly to $\sim$500 keV at $A = 228$ and then presents a further jump to $\sim$700 keV at $A = 230$. Within the framework of the RASM the parity splitting is strongly related to the octupole deformation, even a small change of the octupole deformation will lead to a significant variation of the parity splitting. It is seen from Table I that the octupole deformations for ^{222,224,226}Ra have a similar value, $\epsilon_3 = 0.071$, and this is eventually responsible for the similarity of the parity splittings for these three nuclei. There exists a

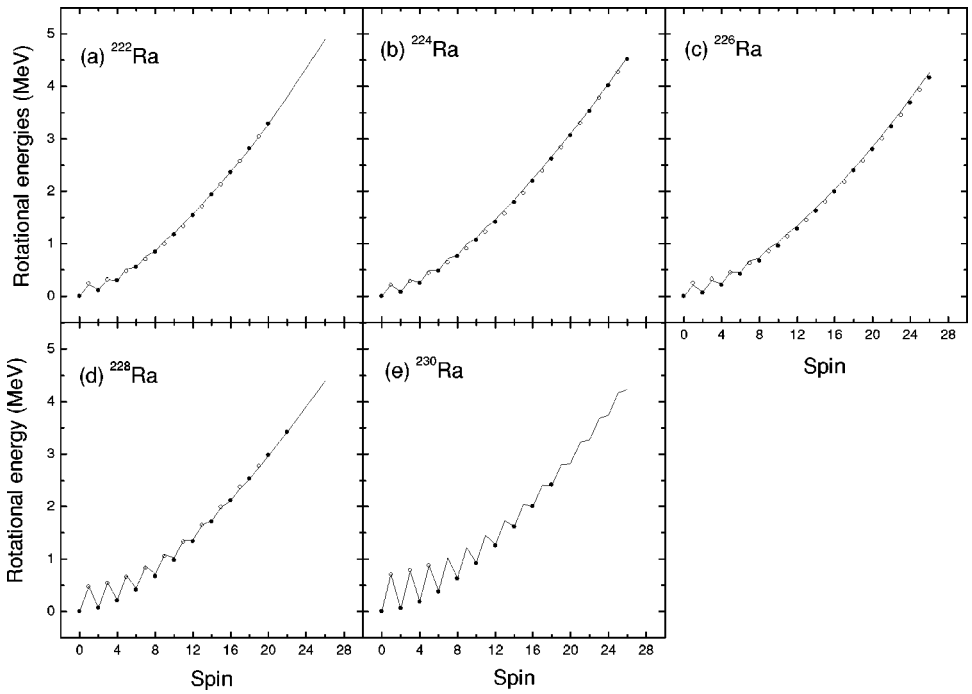

FIG. 2. The calculated yrast rotational bands (solid lines), the energy versus spin, with the deformation parameters listed in Table I for (a) ^{222}Ra, (b) ^{224}Ra, (c) ^{226}Ra, (d) ^{228}Ra, and (e) ^{230}Ra, are compared with the experimental data (open circles for negative and solid circles for positive parities) taken from Ref. [9].

sudden decrease in the octupole deformation from ^{226}Ra to ^{228}Ra, ϵ_3 changing from 0.071 to 0.061, this is the origin of the big jump of the parity splitting at $A=228$ shown in Fig. 3. A further decrease of the octupole deformation to $\epsilon_3=0.055$ for ^{230}Ra seems to be the reason for the second rising of the parity splitting at $A=230$. It is noteworthy from the present calculations that the parity splitting is a sensitive measure of the extent to which the system has the reflection asymmetry. The decrease of the octupole deformation from ^{226}Ra to ^{228}Ra is actually implied by the measurements of the intrinsic $E1$ moments D_0 of these two nuclei, which are larger, 0.06–0.1 e fm, for ^{226}Ra [15] and smaller, 0.011 e fm, for ^{228}Ra [16] at low spins. The change of the octupole deformation is also transparent by examining the level structure of the single particle states calculated with an octupole deformed WS potential, which shows the pronounced energy gap of neutron number $N=138$ at around $\epsilon_3=0.08$ [14]. The gap feature of the single particle spectra ensures that the shell effects favor a larger octupole deformation for ^{226}Ra ($N=138$) than for ^{228}Ra ($N=140$) and ^{230}Ra ($N=142$).

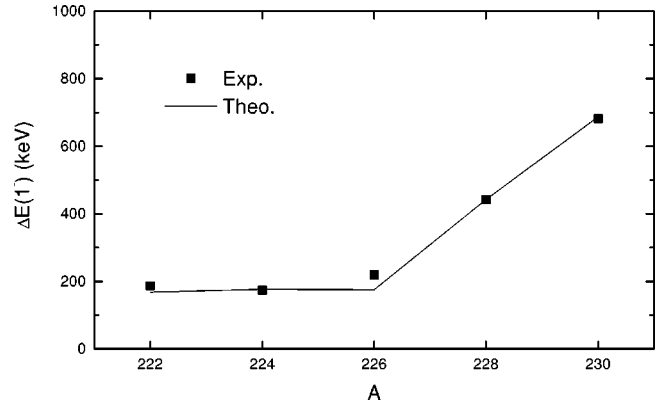

FIG. 3. The calculated parity splittings (line) at spin 1^- for the Ra isotopes are plotted versus the mass number and compared with the experimental data (solid square). Both the calculated and the experimental splittings are taken from Fig. 2.

The parity splitting of rotational octupole bands may be quenched due to fast rotation and there exists an approximate critical spin I_c where the splitting vanishes and the negative and positive states become perfectly interleaved according to the energy formula $E_I \sim I(I+1)$. By viewing the experimental data of the yrast octupole bands one finds that the I_c is about $10\hbar$ for ^{222,224,226}Ra and $18\hbar$ for ^{228}Ra. It is shown in Fig. 2 that these experimental critical spin values are reproduced by the calculations. Again the large increase of the critical spin I_c from ^{226}Ra to ^{228}Ra is attributed to the decrease of the octupole deformation when the neutron number varies from $N=138$ to 140. The present calculation for ^{230}Ra predicts a very large critical spin $I_c>26\hbar$, but unfortunately for this nucleus the negative-parity band has been measured only up to spin $7\hbar$ and the positive parity band only up to $18\hbar$. It would be interesting to extend the measurements of the bands up to higher spins for ^{230}Ra to examine the possible disappearing of the interleaved structure of the alternating parity states which were observed in all the lighter Ra isotopes.

V. SUMMARY

In summary, the reflection asymmetric shell model has been formulated to describe the high spin states of octupole deformed nuclei. The long-range separable forces of quadrupole, octupole, and hexadecapole as well as monopole and quadrupole pairing are included in the Hamiltonian. The shell model space is spanned by the eigenstates of angular momentum and parity obtained by projecting the intrinsic octupole deformed BCS multiquasiparticle states onto both

good angular momentum and good parity. The observed yrast octupole bands have the common features which differ from those of normal rotational bands observed in nonoctupole but deformed nuclei. All these general striking features characteristic of an octupole deformed nuclear system can be interpreted and reproduced by the RASM. The present calculations of the yrast octupole bands, the energy versus spin, for ^{222,224,226,228,230}Ra are in good agreement with the experimental data. Within the framework of the RASM the observed sudden increase of the parity splitting at low spins from ^{226}Ra ($N=138$) to ($N=140$) may be interpreted by the significant decrease of the octupole deformation for ^{228}Ra. It has been demonstrated by the calculations that the RASM is a useful model to explore into the nuclear reflection asymmetry.

ACKNOWLEDGMENTS

Stimulating discussions with Y. Sun are gratefully acknowledged. This work is supported by the National Natural Science Foundation of China under Contract Nos. 19935030, 10075078, 10047001, and by the Major State Basic Research Development Program of China under Contract No. G20000774.

[1] F. Asaro, F.S. Stephens, Jr., and I. Perlman, Phys. Rev. **92**, 1495 (1953).
[2] F.S. Stephens, Jr., F. Asaro, and I. Perlman, Phys. Rev. **100**, 1543 (1955).
[3] J. Fernandez-Niello *et al.*, Nucl. Phys. **A391**, 221 (1982).
[4] D. Ward *et al.*, Nucl. Phys. **A406**, 591 (1983).
[5] I. Ahmad and P.A. Butler, Annu. Rev. Nucl. Part. Sci. **43**, 321 (1993).
[6] P.A. Butler and W. Nazarewicz, Rev. Mod. Phys. **68**, 349 (1996).
[7] J.F. Smith *et al.*, Phys. Rev. Lett. **75**, 1050 (1995).
[8] J.F.C. Cocks *et al.*, Phys. Rev. Lett. **78**, 2920 (1997).
[9] J.F.C. Cocks *et al.*, Nucl. Phys. **A645**, 61 (1999).
[10] W. Nazarewicz and P. Olanders, Nucl. Phys. **A441**, 420 (1985).
[11] J.P. Elliott, Proc. R. Soc. London **245**, 128 (1968); **245**, 557 (1968).
[12] K. Hara and S. Iwasaki, Nucl. Phys. **A332**, 61 (1979).
[13] K. Hara and Y. Sun, Int. J. Mod. Phys. E **4**, 637 (1995).
[14] G.A. Leander and Y.S. Chen, Phys. Rev. C **37**, 2744 (1988).
[15] H.J. Wollersheim *et al.*, Nucl. Phys. **A556**, 261 (1993).
[16] E. Ruchowska *et al.*, Nucl. Phys. **A383**, 1 (1982).
[17] N.V. Zamfir, P. von Brentano, and R.F. Casten, Phys. Rev. C **49**, R605 (1994).
[18] I. Wiedenhover *et al.*, Phys. Rev. Lett. **83**, 2143 (1999).